ADVANCED MATERIALS

DOI: 10.1002/adma.200701514

Potassium Tungsten Bronze Nanowires: Polarized Micro-Raman Scattering of Individual Nanowires and Electron Field Emission from Nanowire Films

By *Zhe Zheng*, *Bin Yan*, *Jixuan Zhang*, *Yumeng You*, *Chwee Teck Lim*, *Zexiang Shen*, and *Ting Yu**

Nanostructures are known to possess large surface-area-to-volume ratios and possible quantum-confinement effects. They have currently been intensely researched because these special properties can give rise to potential applications in nanotechnology,[1] such as the fabrication of nanometer-scale devices.[2] In the family of nanostructures, metal oxide nanostructures have significantly been applied in areas such as chemical/biological sensing, lasering, and displays,[1] and are the most important and widely studied nanostructures. Many methods have been developed for the fabrication of nanostructures, including applying electrochemical techniques,[3] porous aluminum templates,[4] vapor–liquid–solid (VLS) growth[5] and vapor–solid (VS) reactions.[6] Heat-oxide methods have been shown to provide an alternative route for synthesis of metal oxide semiconductor (MOS) nanostructures, with the advantages of mild synthetic conditions, simple manipulation, and large-scale production.[7] The hotplate method, one of the simplest heat-oxide methods in particular, has been successfully applied for the synthesis of various metal oxide (CuO, α-Fe_2O_3, Co_3O_4, and ZnO) nanostructures.[7-10]

In the past few decades, much attention has been focused on tungsten bronzes owing to their Drude-type optical behavior,[11] photochromic,[12] and superconducting properties.[13] In particular, the hexagonal alkali tungsten bronzes A_xWO_3 (HTBs, A = K, Rb, Cs, and NH_4; $0 < x < 1/3$) have been the subject of numerous studies.[14,15] The traditional methods for the preparation of the hexagonal tungsten bronze structure require high temperature reaction of metal tungstate, tungsten oxide, and metal tungsten powder[16] or the electrochemical reduction of tungstate.[17] Here, we demonstrate a simple and convenient process for the synthesis of $K_{0.33}W_{0.944}O_3$ nanowires. Our scanning electron microscopy (SEM) investigations directly confirm that the growth mechanism is that of the tip-growth vapor–solid mechanism. Raman scattering is a well-established technique for elucidating structural properties of nanostructures. More recently, micro-Raman studies on individual nanowires such as SiC,[18] ZnSe,[19] and CuO[8] successfully demonstrate their impressive potential for probing crystal properties of basic building blocks such as single nanowires. However, to the best of our knowledge, there is no polarized micro-Raman scattering study on individual potassium tungsten bronze nanowires to date. For the first time, the electron field emission measurement of potassium tungsten bronze nanowire film was performed in this work.

A field-emission scanning electron microscope (FE-SEM) was used to directly observe the morphology of the as-grown samples. After being heated at 450 °C for 10 hours in air, the pretreated tungsten foil was found to be covered with a layer of randomly oriented nanowires with diameters and lengths in the range of approximately 50–200 nm and 5–10 μm (Fig. 1a), respectively. The highest aspect ratio was established to be 100, and the average aspect ratio of these nanowires was around 50, which may give rise to promising field-emission properties. It was noted that the tungsten bronze nanostructures are able to be synthesized into nanorods, nanowires, or nanosheets by changing the heating temperatures. The detailed morphology-controlled synthesis of potassium doped tungsten bronze nanostructures will be discussed in our future work. Figure 1b shows the XRD pattern of the as-prepared samples. All the reflections can be indexed to the hexagonal potassium tungsten bronze $K_{0.33}W_{0.944}O_3$ (Joint Comittee on Powder Diffraction Standards (JCPDS) file No. 81-0005) and no impurities were identified in the XRD pattern.

The crystal structural characterization of nanowires was performed by means of high-resolution transmission electron microscopy (HRTEM). The fringe spacing of 0.38 nm (Fig. 2b) concurs well with the interplanar spacing of (0 0 1) plane of hexagonal $K_{0.33}W_{0.944}O_3$ (JCPDS file No. 81-0005), revealing the single crystalloid of the synthesized tungsten bronze nanowires and the growth direction of [0 0 1]. The selected area electron diffraction (SAED) pattern with the zone axis $[0\bar{2}0]$ (inset of Fig. 2a) further confirmed the single crystalline property of nanowires. The ideal hexagonal symmetry structure of A_xWO_3 (A = K, Rb, and Cs) is schematically shown in the inset of Figure 2c. The WO_6 octahedra are formed into a six-member ring. Consequently, the maximum alkali-metal content is 0.33 if the composition ratio of W is set to be 1.[20] The

[*] Z. Zheng, B. Yan, Y. M. You, Prof. Z. X. Shen, Dr T. Yu
Division of Physics and Applied Physics
School of Physical and Mathematical Sciences
Nanyang Technological University
Singapore 637371 (Singapore)
E-mail: yuting@ntu.edu.sg
Dr J. X. Zhang, Prof. C. T. Lim
Department of Mechanical Engineering, Division of Bioengineering
Department of Materials Science & Engineering
National University of Singapore
9 Engineering Drive 1, Block EA, Singapore 117576 (Singapore)

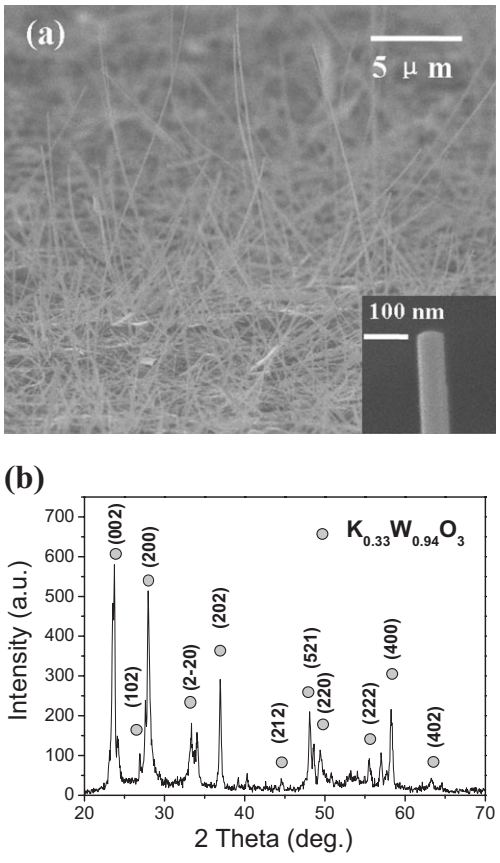

Figure 1. a) SEM image of the as-prepared sample with heating temperature of 450 °C and duration of 10 h. The inset shows high resolution SEM image of the $K_{0.33}W_{0.944}O_3$ single nanowire. b) XRD pattern of the as-prepared sample.

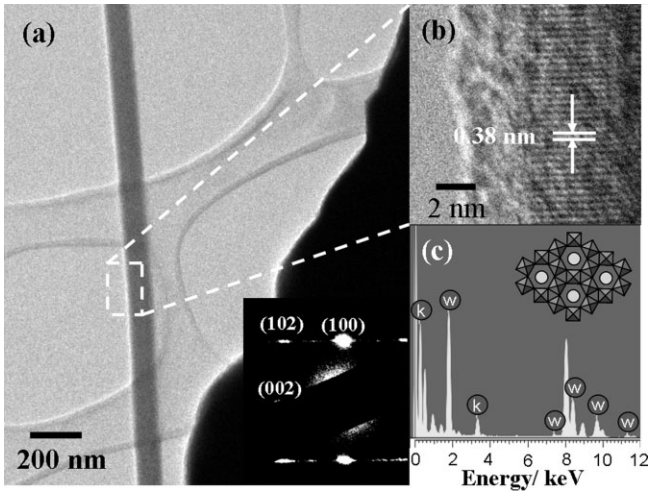

Figure 2. a) TEM image of the $K_{0.33}W_{0.944}O_3$ nanowire. The inset of (a) shows the selected area electron diffraction (SAED) pattern (circled region) of nanowires which indicates good agreement with the diffraction pattern of $K_{0.33}W_{0.944}O_3$ from the zone axis of $[0\bar{2}0]$. b) HRTEM image of the nanowires. c) EDS data for the hexagonal $K_{0.33}W_{0.944}O_3$ nanowire. The inset of (c) shows arrangement of $[WO_6]$ octahedral in the structure of hexagonal $K_{0.33}W_{0.944}O_3$. Potassium ions occupy these hexagonal channels.

elemental ratio between potassium and tungsten along the nanowires was investigated by recording the energy dispersive X-ray spectra (EDS) of nanowires from one end to the other during the TEM measurement. The sample spectrum is shown in Figure 2c. The average ratio of K/W among different nanowires is equal to 0.36, which is in good agreement with the XRD and TEM results that the nanowires are hexagonal potassium tungsten bronze, $K_{0.33}W_{0.944}O_3$. The deviation may indicate the existence of more W atom vacancies in our nanowires as compared with $K_{0.33}W_{0.944}O_3$.

Figure 3a shows the schematic diagram of the setup for polarized micro-Raman scattering investigation on an individual $K_{0.33}W_{0.944}O_3$ nanowire (optical image shown in Fig. 3b). The x-axis is set to coincide with the *c*-axis of the hexagonal structure, which is also the long-axis of the nanowires. By rotating

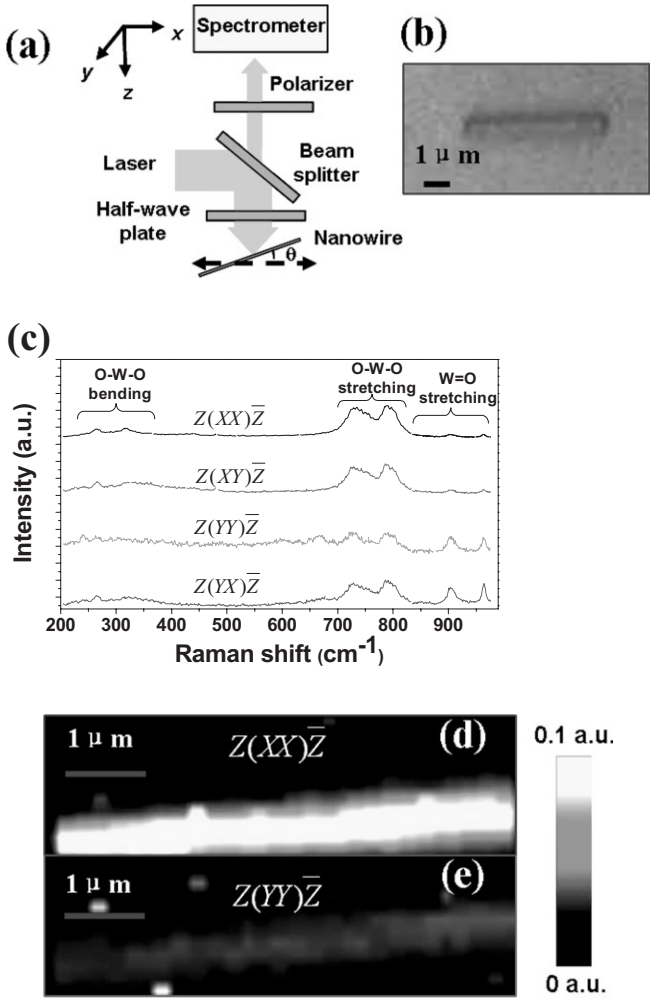

Figure 3. a) Schematic diagram of the setup for the polarized Raman scattering characterization, b) optical image of individual $K_{0.33}W_{0.944}O_3$ nanowire, c) polarized Raman spectra of the nanowire shown in (b) (all peaks were normalized to the strongest peak located at 790 cm^{-1}), and d,e) Raman mapping images of the nanowire shown in (b) by plotting the intensity ratio between the W=O stretching bands to the O–W–O stretching bands with different polarization geometries as illustrated.

ADVANCED MATERIALS

the half-wave plate, the polarization of the incident laser beam is able to be tuned with respect to the long-axis of the nanowires. The polarized Raman signals are distinguished by a polarizer. As shown in Figure 3c, there are three groups of Raman peaks in the regions of 900–980, 600–850, and 200–400 cm^{-1}, which could be assigned to W=O stretching, O–W–O stretching and O–W–O bending modes, respectively.[21] The appearance of the two Raman bands in the 900–980 cm^{-1} region may indicate the presence of terminal W=O bonds, which may support our previous speculation that the nanowires contain W atom vacancies.[21] According to the relationship between the wave number (ν) of a Raman-active W=O stretching mode with bond length (d): $\nu = 25823 \exp(-1.902d)$,[22] the lengths of the corresponding W=O bonds were estimated to be 1.728 and 1.764 Å. Moreover, it is worth to note the bandwidth of the Raman mode of around 960 cm^{-1} is quite small (ca. 7 cm^{-1}), which may suggest that the W vacancies are arranged in order. The polarization measurements (Fig. 3c) clearly show that both the O–W–O and the W=O stretching modes are sensitive to the polarization of the incident laser beam. When the E field of laser is parallel to the nanowire, the O–W–O stretching bands are much stronger than the W=O stretching bands, while the latter significantly increase and become comparable with the former when there is a 90° angle between the polarization of the laser and the nanowire. The intensity of W=O stretching bands is about five times more intense in the $Z(YY)\bar{Z}$ polarization than that in the $Z(XX)\bar{Z}$ polarization. The apparent polarization dependence of Raman modes observed here is very similar with the results of the single crystal hexatungstates[21] and effectively demonstrates the monocrystalline of our potassium tungsten bronze nanowires. To further determine whether the whole nanowires are single crystalline or not, the polarized Raman mapping was performed. Figure 3 shows the polarized Raman mapping images of the nanowire with different polarization geometries as illustrated. The Raman images were plotted based on the ratio of the intensity of the W=O stretching bands over the O–W–O stretching bands. Besides the different contrast due to the different polarization despondences, both two images appear as a uniform contrast distribution along the entire nanowire. The absence of any local polycrystalline domain which exhibits unpolarized dependence readily shows that the nanowire is one piece of single crystal with high quality.

In contrast with previous work,[23,24] where the vapor–liquid–solid (VLS) mechanism was employed to explain the growth of tungsten bronze nanowires, here we attributed our growth mechanism to the vapor–solid (VS) mechanism as with careful observation, we failed to see any catalyst particles attached on the nanowires in both the TEM and SEM images. Vapor-based mechanisms have been intensely studied and widely used to explain the growth of tungsten bronze and tungsten oxide nanowires. [23, 24] However, the growth taking place at tip or root of nanowires is still unknown. To elucidate this issue, dynamic growth process of a specific individual nanowire was monitored by SEM. As shown in Figure 4, the

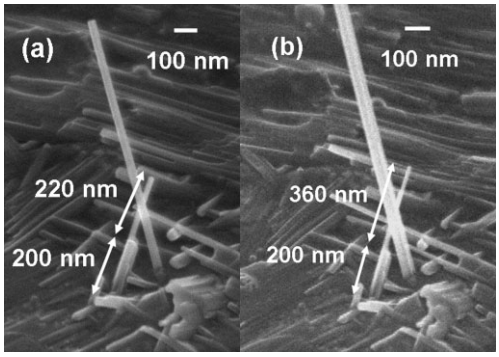

Figure 4. a) SEM image of the as-prepared sample with a heating temperature of 450 °C and duration of 1 h. b) SEM image of the nanowires in (a) after being heated for an additional hour at 450 °C.

further heating process only caused the increase of the length of the top narrow part while the bottom part remains the same length. The continuous growth with the absence of particle at the tip further supports the VS mechanism. Therefore, we proposed that the growth mechanism in this work is tip-growth VS mechanism. Crystalline (the XRD pattern and Raman spectrum are not shown here) mixtures consisting of W–K–O compounds such as $K_{0.33}WO_3{\cdot}22H_2O$, which may be obtained from the reaction between W and KOH solution, was observed on the W foil after it was sonicated in KOH solution and dried in air. Upon heating, the tungsten bronze hydrate released the water molecules of the crystal water in its crystalline framework and initiated evaporation. Once the vapor reached supersaturation, the nucleation of $K_{0.33}W_{0.944}O_3$ at the top layer of substrate occurred. The continuous nucleation along the energetically favorable direction, such as [001] caused the growth of short nanorods. The subsequent growth of nanowires then resulted from accumulation of the molecules at the tip of nanorods until the source was used up or the heating process had stopped. Another possible channel which might have contributed to the tungsten bronze vapor is the reaction between W and KOH, as proposed earlier.[21]

Field emission measurements were performed using a diode structure with indium tin oxide (ITO)-coated quartz as the anode and tungsten foil with tungsten bronze nanowires as the cathode. The inter-electrode, i.e., cathode to anode distance (D), was maintained at 100 μm and the experiments were conducted at 5.1×10^{-7} mbar (around 3.8×10^{-7} Torr). Figure 5a gives the typical current density–electric field (J–E) curve of the $K_{0.33}W_{0.944}O_3$ nanowire films. It shows a low turn-on field of 7 V μm^{-1} and a large current density of 1.4 mA cm^{-2} with the field of 11 V μm^{-1}. In this experiment, the turn-on field is defined by the emission current achieving 10 μA cm^{-2}. The exponential dependence between the emission current and the applied field, plotted by the $\ln(J/E^2) \sim 1/E$ relationship (inset of Fig. 5a), indicates that the field emission from $K_{0.33}W_{0.944}O_3$ nanowire films follows the Fowler–Nordheim (FN) relationship.[25] The dots are experimental data and the solid line is the fitting curve in accordance to the simplified Fowler–Nordheim equation

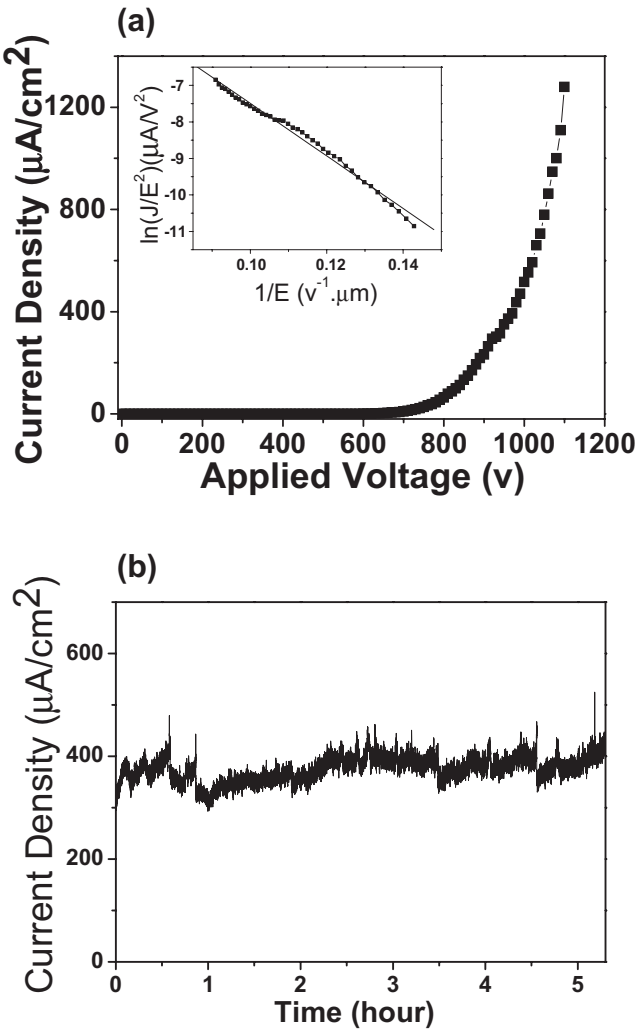

Figure 5. a) Typical field-emission current–voltage (*I–V*) curves of $K_{0.33}W_{0.944}O_3$ nanowire films. The inset shows the F-N plots ($\ln(J/E^2)$ vrsus $1/E$) accordingly, which exhibits a good linear dependence. b) Long-term stability measurement of field emission property of nanowire films shown in Fig. 1a.

$$J = \frac{A(\beta E)^2}{\varphi} \exp\left[\frac{-B\varphi^{\frac{3}{2}}}{\beta E}\right] \quad (1)$$

where J is the current density, E is the local field strength, φ is the work function, for electron emission, which is estimated to be 1.76 eV[26] for $K_{0.33}W_{0.944}O_3$, A and B are constants with the value of 1.54×10^{-6} A V^{-2} eV and 6.83×10^7 V cm^{-1} eV$^{-3/2}$,[25] respectively. Here, due to the large aspect ratio of nanowires, E is usually much stronger than the "applied field", E_{appl}, β is the field enhancement factor, which is defined by

$$E = \beta E_{appl} = \beta \frac{V}{d} \quad (2)$$

where E is the local electric field near the emitter tip and β is a parameter depending on the aspect ratio of the nanostructures, crystal structures, and the density of the emitting points, d is the average spacing between the electrodes (d = 100 μm in this work), and V is the applied voltage. β was obtained to be 221 from the linear fitting of the F–N curve at turn-on area and the maximum emission current density of 1.4 mA cm^{-2} is obtained under a voltage of 1.1 kV. Compared with the AlN nanoneedles[27] and the ZnO nanopins,[28] such an enhancement factor is acceptable for application, although much lower than that of carbon nanotubes.[29] The reasons for this low enhancement factor could be the random alignment of the nanowires (Fig. 1a). The field emission stability of the $K_{0.33}W_{0.944}O_3$ nanowire film sample was investigated and the typical results are shown in Figure 5b. The total emission current was monitored over time under an applied macroscopic field of 9 V μm^{-1} and an emitter–anode gap of 100 μm. At an emission current density of ca. 350 μA cm^{-2}, the fluctuations were less than 5 % and no degradations were observed. To the best of our knowledge, this is the first time that the field emission properties of tungsten bronze nanowires were measured.

In conclusion, single-crystalline $K_{0.33}W_{0.944}O_3$ nanowires have been synthesized using a rather simple method at a low temperature of 450 °C in air. The vapor–solid (VS) mechanism with tip growth process was proposed. The single crystallinity of nanowires has also been demonstrated by polarized Raman mapping on individual nanowires. The electron field emission investigations demonstrated the promising properties of the $K_{0.33}W_{0.944}O_3$ nanowire films. With further improvements, potassium tungsten bronze nanostructures can become one of the potential candidates for use in future field emission electron sources and displays (FEDs).

Experimental

Fresh tungsten foils (10 mm × 10 mm × 0.25 mm) with a purity of 99.9% (Aldrich) were used as both reagents and substrates for the growth of potassium tungsten bronze nanostructures. After having been polished and cleaned, tungsten foils were sonicated in the potassium hydroxide solution (0.05 mol dm^{-3}). The tungsten foil was then heated on a hotplate under ambient conditions after it had been dried naturally. The growth temperature and duration were fixed at 450 °C and 10 h, respectively. The morphologies of the as-prepared products were examined by SEM (JEOL JSM-6700F) for the analysis of topographical morphologies while the compositions of the top layer of the samples were characterized by X-ray diffraction (XRD) (Bruker D8 with Cu K_α irradiation) and micro-Raman spectroscopy (Witech CRM200, λ_{laser} = 532 nm). TEM (JEOL JEM 2010F, 200 kV) was used to investigate the crystal structure of the different nanostructure products while the energy dispersive X-ray spectrometry (EDS) incorporated into the TEM chamber was used to determine the elemental composition of nanowires. Field-emission measurement was carried out in a vacuum chamber with a pressure of 3.8×10^{-7} Torr at room temperature under a two-parallel-plate configuration. Details of the measurement system and procedure were reported previously [30].

Received: June 25, 2007
Revised: August 24, 2007
Published online: January 3, 2008

[1] Y. Xia, P. Yang, Y. Sun, Y. Wu, B. Mayers, B. Gates, Y. Yin, F. Kim, H. Yan, *Adv. Mater.* **2003**, *15*, 353.
[2] Z. L. Wang, *Adv. Mater.* **2000**, *12*, 1295.
[3] Y. Zhou, S. H. Yu, X. P. Cui, C. Y. Wang, Z. Y. Chen, *Chem. Mater.* **1999**, *11*, 545.
[4] X. Y. Zhang, L. D. Zhang, Y. Lei, L. X. Zhao, Y. Q. Mao, *J. Mater. Chem.* **2001**, *11*, 1732.
[5] X. F. Duan, C. M. Lieber, *Adv. Mater.* **2000**, *12*, 298.
[6] J. Y. Lao, J. Y. Huang, D. Z. Wang, Z. F. Ren, *Nano Lett.* **2003**, *3*, 235.
[7] T. Yu, Y. W. Zhu, X. J. Xu, Z. X. Shen, P. Chen, C. T. Lim, J. T. L. Thong, C. H. Sow, *Adv. Mater.* **2005**, *17*, 1595.
[8] T. Yu, X. Zhao, Z. Shen, Y. Wu, W. Su, *J. Cryst. Growth* **2004**, *268*, 590.
[9] T. Yu, Y. W. Zhu, X. J. Xu, K. S. Yeong, Z. X. Shen, P. Chen, C. T. Lim, J. T. L. Thong, C. H. Sow, *Small* **2006**, *2*, 80.
[10] Y. W. Zhu, C. H. Sow, T. Yu, Q. Zhao, P. H. Li, Z. X. Shen, D. P. Yu, J. T. L. Thong, *Adv. Funct. Mater.* **2006**, *16*, 2415.
[11] S. K. Deb, *Appl. Opt. Suppl.* **1969**, *3*, 192.
[12] S. Reich, Y. Tsabba, *Eur. Phys. J.* **1999**, *B9*, 1.
[13] L. H. Cadwell. R. C. Morris, W. G. Moulton, *Phys. Rev. B* **1981**, *23*, 2219.
[14] T. Kudo, A. Kishimoto, H. Inoue, *Solid State Ionics* **1990**, *40–41*, 567.
[15] M. S. Whittingham, in *Solid State Device* (Eds: B. V. R. Chowdari, S. Radhakrishnan), World Scientific, Singapore, **1988**.
[16] L. D. Muhlestein, G. C. Danielson, *Phys. Rev.* **1967**, *158*, 825.
[17] S. V. Vakarin, A. N. Baraboshkin, K. A. Kaliev, V. G. Zyrianov, *J. Cryst. Growth* **1995**, *151*, 121.
[18] M. Bechelany, A. Brioude, D. Cornu, G. Ferro, P. Miele, *Adv. Mater.* **2007**, *17*, 939.
[19] C. X. Shan, Z. Liu, X. T. Zhang, C. C. Wong, S. K. Hark, *Nanotechnology* **2006**, *17*, 5561.
[21] Z. Gu, Y. Ma, T. Zhai, B. Gao, W. Yang, J. Yao, *Chem. Eur. J.* **2006**, *12*, 7717.
[22] M. Maczka, J. Hanuza, A. Wáskowska, *J. Raman Spectrosc.* **2003**, *34*, 432.
[23] F. D. Hardcastle, I. E. Wachs, *J. Raman Spectrosc.* **1995**, *26*, 397.
[24] G. Gu, B. Zheng, W. Q. Han, S. Roth, J. Liu, *Nano Lett.* **2002**, *2*, 849.
[25] H. Qi, C. Wang, J. Liu, *Adv. Mater.* **2003**, *15*, 411.
[26] R. Fowler, L. W. Nordheim, *Proc. R. Soc. London Ser. A* **1928**, *119*, 173.
[27] F. Zocchi, *Z. Nat. Forsch. A J. Phys. Sci.* **1989**, *44*, 87.
[28] Q. Zhao, J. Xu, X. Y. Xu, Z. Wang, D. P. Yang, *Appl. Phys. Lett.* **2005**, *85*, 5331.
[29] C. X. Xu, X. W. Sun, *Appl. Phys. Lett.* **2003**, *83*, 3806.
[30] I. Alexandrou, E. Kymakis, G. A. J. Amaratunga, *Appl. Phys. Lett.* **2002**, *80*, 1435.
[31] Y. W. Zhu, T. Yu, F. C. Cheong, X. J. Xu, C. T. Lim, V. B. C. Tan, J. T. L. Thong, C. H. Sow, *Nanotechnology* **2005**, *16*, 88.

